Comparative analysis of deformable mirrors for ocular adaptive optics

Eugenie Dalimier and Chris Dainty

Applied Optics Group, Department of Experimental Physics, National University of Ireland, Galway, Ireland

eugenie.dalimier@nuigalway.ie

Abstract: We have evaluated the ability of three commercially available deformable mirrors to compensate the aberrations of the eye using a model for aberrations developed by Thibos, Bradley and Hong. The mirrors evaluated were a 37 actuator membrane mirror and 19 actuator piezo mirror (OKO Technologies) and a 35 actuator bimorph mirror (AOptix Inc). For each mirror, Zernike polynomials and typical ocular aberrated wavefronts were fitted with the mirror modes measured using a Twyman-Green interferometer. The bimorph mirror showed the lowest root mean square error, although the 19 actuator piezo device showed promise if extended to more actuators. The methodology can be used to evaluate new deformable mirrors as they become available.

OCIS codes: (010.1080) Adaptive optics; (230.3990) Microstructures devices; (330.4460) Ophthalmic optics

References and links

1. J. Liang and D. R. Williams, "Aberrations and retinal image quality of the normal human eye," J. Opt. Soc. Am. A **14**, 2873–2883 (1997).
2. J. Liang, D. R. Williams, and D. T. Miller, "Supernormal vision and high-resolution retinal imaging through adaptive optics," J. Opt. Soc. Am. A **14**, 2884–2892 (1997).
3. M. Glanc, E. Gendron, F. Lacombe, D. Lafaille, J.-F. L. Gargasson, and P. Léna, "Towards wide-field retinal imaging with adaptive optics," Opt. Commun. **230**, 225–238 (2004).
4. N. Doble, G. Y. Yoon, L. Chen, P. Bierden, B. Singer, S. Oliver, and D. R. Williams, "Use of a microelectromechanical mirror for adaptive optics in the human eye," Opt. Lett. **27**, 1537–1539 (2002).
5. E. J. Fernández and P. Artal, "Membrane deformable mirror for adaptive optics: performance limits in visual optics," Opt. Express **11**, 1056–1069 (2003).
6. L. Diaz-Santana, C. Torti, I. Munro, P. Gasson, and C. Dainty, "Benefit of higher closed-loop bandwidths in ocular adaptive optics," Opt. Express **11**, 2597–2605 (2003).
7. F. Vargas-Martín, P. M. Prieto, and P. Artal, "Correction of the aberrations in the human eye with a liquid-crystal spatial light modulator: limits to performance," J. Opt. Soc. Am. A **15**, 2552–2562 (1998).
8. L. N. Thibos, A. Bradley, and X. Hong, "A statistical model of the aberration structure of normal, well-corrected eyes," Ophthal. Physiol. Opt. **22**, 427–433 (2002).
9. M. K. Smolek and S. D. Klyce, "Zernike Polynomial Fitting Fails to Represent All Visually Significant Corneal Aberrations," Invest. Ophthalmol. Visual Sci. **44**, 4676–4681 (2003).
10. F. Roddier, *Adaptive optics in astronomy*, 1st ed. (Cambridge University Press, Cambridge, U.K., 1999).
11. G. Vdovin and P. M. Sarro, "Flexible mirror micromachined in silicon," Appl. Opt. **34**, 2968–2972 (1995).
12. C. Paterson, I. Munro, and J. C. Dainty, "A low cost adaptive optics system using a membrane mirror," Opt. Express **6**, 175–185 (2000).
13. D. A. Horsley, H. K. Park, S. P. Laut, and J. S. Werner, "Characterization for vision science applications of a bimorph deformable mirror using phase-shifting interferometry," in *Ophthalmic Technologies XV*, F. Manns, P. G. Sderberg, A. Ho, B. E. Stuck, and e. M. Belkin, eds., Proc. SPIE **5688**, 133–144 (2005).
14. L. N. Thibos, R. A. Applegate, J. T. Schwiegerling, and R. Webb, "Standards for reporting optical aberrations of eyes," J. Refract. Surg. **18**, 652–660 (2000).

#7336 - $15.00 US
Received 3 May 2005; revised 23 May 2005; accepted 23 May 2005

15. L. N. Thibos, X. Hong, A. Bradley, and X. Cheng, "Statistical variation of aberration structure and image quality in a normal population of healthy eyes," J. Opt. Soc. Am. A **19**, 2329–2348 (2002).
16. K. M. Hampson, "The higher-order aberrations of the human eye: relation to the pulse and effect on vision," Ph.D. thesis, Imperial College, London (2004).
17. E. Dalimier, K. M. Hampson, and J. C. Dainty, "Effects of adaptive optics on visual performance," in *Imaging and Vision*, e. Fionn D. Murtagh, ed., Proc. SPIE **5823** (2005).

1. Introduction

Adaptive optics (AO) was first implemented to correct higher-order ocular aberrations by Liang *et al.* in 1997 [1, 2]. Since then, several systems have been built around the world, mostly dedicated to high-resolution imaging, but also to investigate the effects of higher-order aberrations of the eye on visual performance. During these years, new wavefront correction technologies have been considered and implemented. The initial system described by Liang *et al.* comprised a piezo-electric device originally developed for astronomical purposes by Xinetics (Devens, MA, USA). Similarly, Glanc *et al.* [3] obtained corrected retinal images with a bimorph mirror designed for astronomy. However, the need for more compact and economic devices was clear from the beginning. New micromachining technologies were enabling the batch fabrication of inexpensive products. The difficulty was to obtain such a corrective device that would still have sufficient stroke to correct the aberrations of the human eye. It was shown that a microelectromechanical (MEMS) mirror, manufactured by Boston Micromachines (Watertown, MA, USA) could provide a correction [4] comparable to that obtained with the Xinetics mirror. The high resolution retinal images presented by Hofer *et al.* could then be expected to be repeated with micromachined mirrors. Nevertheless, the closed-loop systems implementing bulk micromachined deformable mirrors, like the membrane OKO Technologies (Delft, The Netherlands) mirror, have demonstrated a good correction [5, 6] but no retinal images have been displayed. Meanwhile, other studies have investigated the use of other devices. Vargas *et al.* [7] demonstrated the use of liquid-crystal spatial light modulators while highlighting their application limited to a static and monochromatic correction.

We compare here three different mirrors, of which two have only recently become commercially available. These two mirrors are actuated with technologies already mentioned, namely piston-like piezo-electric (the OKO 19 actuators mirror) and bimorph (the AOptix mirror) technology, but they were manufactured in a more compact way. The evaluation of the ability to correct ocular aberrations is usually based on the ability of the mirror to generate Zernike polynomials. In addition, we used here typical ocular wavefronts, generated using the Thibos model [8]. Because the Zernike decomposition is not needed in a closed-loop AO correction, and may even fail to represent well ocular aberrations [9], it seemed more appropriate to work directly on the wavefronts.

2. Description of the deformable mirrors

The three mirrors investigated here present different spatial characteristics in terms of optical diameter and actuator geometry, as can be seen in Fig. 1. The optical pupil defines the area over which the spatial characterization was performed. Actuator responses also differ because of the technology used for each mirror. A short description of the three mirrors is given. As the technologies referred to here have been used in astronomy for some time, more details can be obtained from reference books [10].

2.1. The 37 actuator OKO micromachined membrane deformable mirror (MMDM)

This mirror has already been described in several publications, and its behavior has been modelled [11]. It consists of a silicon nitride membrane suspended over an array of electrodes. The

#7336 - $15.00 US Received 3 May 2005; revised 23 May 2005; accepted 23 May 2005

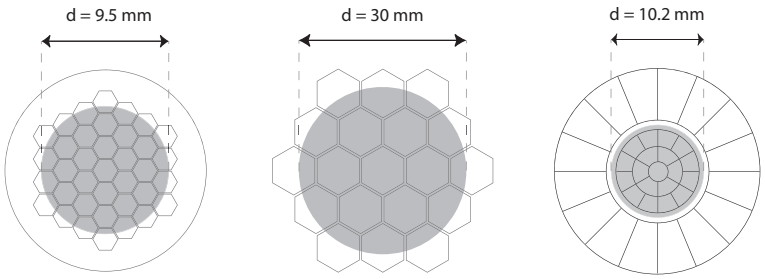

Fig. 1. Actuators layout for the three mirrors considered: the 37ch OKO MMDM , the 19ch OKO, and the 35ch Bimorph. The gray area represents the optical pupil typically used. It is defined as such by the manufacturer for the 19 actuator OKO and the 35 actuator AOptix mirrors, but set by the user for the 37 actuator OKO mirror.

37 electrodes, hexagonally arranged, enable to locally deform the membrane. The membrane is electrostatically attracted towards the electrodes when a voltage is applied to them, as shown in Fig. 2. The surface deformation follows a quadratic dependence on the applied voltage, and

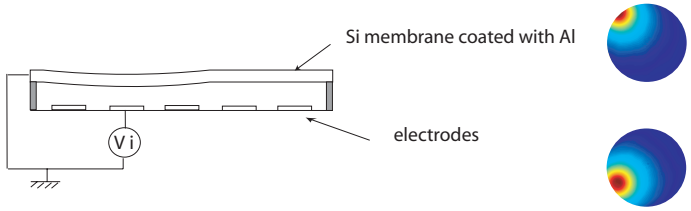

Fig. 2. Schematic of the 37ch OKO mirror actuation and examples of actuator response.

this assumption was used in the performance simulations of the mirror. For the simulations, the optical pupil was reduced to about 2/3 of the mirror diameter, i.e. approximately 9.5 mm as shown in Fig. 1. This is a commonly accepted value, as the membrane is clamped to the edge, and we want to be able to correct for aberrations at the edge of the pupil [12]. The maximum stroke, that is when the maximum voltage is applied to all actuators, was evaluated over this area to 3.5 μm peak-to-valley surface deviation with a commercial Twyman-Green interferometer. The single actuator stroke, corresponding to the maximum voltage applied to one actuator while the others are set to zero, was 500 nm. It should be noted that the mirrors of this series vary in characteristics such as optical flatness and distance between the membrane and the array of electrodes, so that the spatial performance evaluation given here is just an indication of typical performance.

2.2. The 19 actuator OKO piezoelectric deformable mirror

A new 30-mm mirror was recently manufactured by OKO Technologies. It integrates piezoelectric technology into a compact and relatively inexpensive device. The reflective quartz plate has free edge and is piston-like deformed by the lead zirconium titanate (PZT) actuators when a voltage is applied. These features result in sharper influence functions and a larger stroke than the membrane mirror: over the specified voltage range of -150V to 450V, the actuator stroke was evaluated to 3 μm for the 7 inner actuators, and 6/8.5 μm for the outer ring. The reflective plate only covers part of the outer ring of actuators and it is not restricted at the edge, hence it can be deformed to a larger stroke. The mirror behavior was measured over half the specified voltage range, but the values were extrapolated to the full specified range. The actuator

#7336 - $15.00 US
Received 3 May 2005; revised 23 May 2005; accepted 23 May 2005

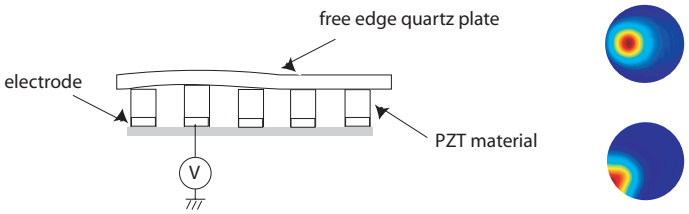

Fig. 3. Schematic of the 19ch OKO mirror actuation and examples of actuator response.

response can be approximated to a linear curve; however the mirror exhibits hysteresis. Over the range 0 to 300V, the hysteresis was measured up to about 14% of the total deformation, as can be seen on Fig. 4. The hysteresis effect was ignored in the present study, since the spatial characterization measurements cancelled it out as explained in Section 3.1.

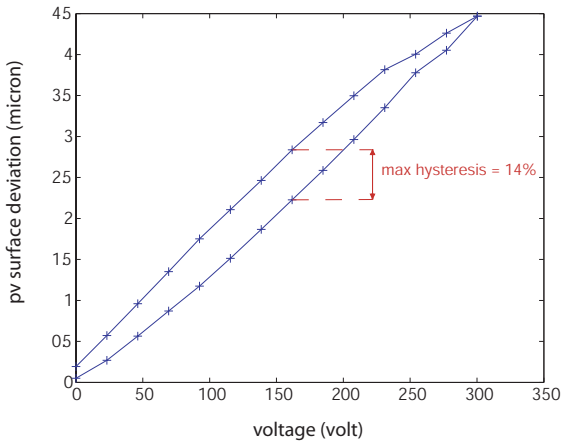

Fig. 4. Measurement of hysteresis through the ramping of one actuator.

2.3. The 35 actuator AOptix bimorph mirror

The AOptix mirror consists of two layers of ceramic lead magnesium niobate (PMN) which are directly actuated by the electrodes bonded on the materials. PMN material deforms when a electric field is applied to it, similarly to PZT, but it differs to it in that the deformation is independent of the polarity of the field, and only 2% hysteresis is present at room temperature (see Fig. 1). The two layers are bonded together with a grounded electrode, and other electrodes

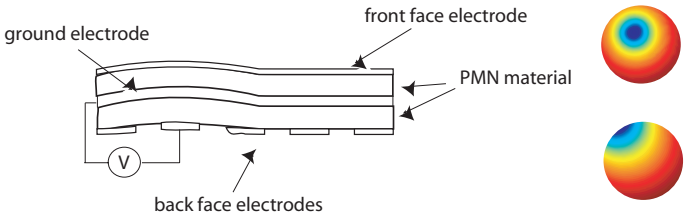

Fig. 5. Schematic of the 35ch AOptix mirror actuation and examples of actuator response.

#7336 - $15.00 US
Received 3 May 2005; revised 23 May 2005; accepted 23 May 2005

are mounted on the back and front face of the mirror. The front face electrode cannot be driven fast due to its high capacitance, hence it is used to produce the overall defocus. A guard ring, which limits the optical pupil, separates the actuators in two groups: the inner actuators produce a curvature deformation while the outer ones are referred to as slope actuators. The total stroke of the mirror is about 16 μm, and the individual stroke of the actuators varies from 3 μm for the 19 inner actuators, and 7 μm for the outer ring of actuators. These values are very similar to those measured on the piezoelectric OKO mirror. The actuator response to the voltage applied is not quite linear, in fact it has been characterized previously [13]. An optimized version of the software corrects for this non-linearity.

3. Phase fitting using the least-square method

The spatial analysis performed over the mirror was based on the least-square fitting of specified phase maps on the mirror. We will describe here the process followed step-by-step and discuss the practical issues.

3.1. Influence functions

The first step was to record each particular deformation produced by the actuators, the so-called influence functions (IF). In order to obtain precise phase maps, a commercial *FISBA* © Twyman-Green interferometer was used. Each phase map was evaluated from the difference of two measurements of the same actuator, and normalized by the range of voltages used. This double measurement is especially important for the 19 actuator OKO, because of the hysteresis issue mentioned earlier. The piston terms, taken as the the average of the values in the images, were removed before all the IFs were stored in a matrix M.

3.2. Principal Components analysis

The IF matrix M contains all the spatial information of the mirror. However, the actuator deformations are by no mean orthogonal. Hence it is necessary to obtain an orthonormal set of wavefronts, over which the deformation produced by any set of commands can be exactly decomposed. These mirror modes are obtained through a singular value decomposition (SVD):

$$M = UWV^T \tag{1}$$

This principal components decomposition defines U and V as orthogonal sets of the mirror modes: U contains the phase maps and V the corresponding command sets. W gives the singular values: the smaller the singular value, the less responsive the mirror and the larger the commands needed to be sent for a unit mode amplitude. We will see later how these singular values are important to avoid clipping of the mirror.

Any phase Φ can be projected on this finite base, and the residual wavefront gives us an evaluation of the fitting efficiency of the mirror. The projection is mathematically expressed by

$$\Phi_M = UU^T\Phi \tag{2}$$

The parameter used to determine the fitting error was the root-mean-square (rms) of the wavefront difference between Φ and Φ_M. It should be noted here that this projection does not take into account the limited range of commands available for the mirror. Hence it is necessary to simultaneously work on the corresponding commands and make sure they remain within the range available. The set of commands c is recovered with the pseudo-inverse M^+, which can be calculated using the SVD:

$$c = M^+\Phi = VW^{-1}U^T\Phi \tag{3}$$

This issue will be discussed in further detail in the next section.

#7336 - $15.00 US Received 3 May 2005; revised 23 May 2005; accepted 23 May 2005

4. Simulation results

4.1. Generation of Zernike polynomials

The Zernike polynomials are widely used to decompose ocular and other wavefronts. Therefore, we started the simulations working on these defined phase maps. For each normalized Zernike polynomial, the corresponding vector of commands was calculated using Eq. (3). It was then rescaled so that the commands would cover half the range of available voltage. Multiplying this new vector by the matrix M again gives the maximum signed best Zernike fit Z_M, meaning that the mirror will be able to produce the phase deformation $\pm Z_M$. This is equivalent to rescaling the projected wavefront

$$Z_M = \frac{c_{lim}}{|c_{max}|} U U^T Z \tag{4}$$

where c_{lim} is the maximum command applicable, and $|c_{max}|$ is obtained as follows:

$$|c_{max}| = max(abs(M^+ Z)) \tag{5}$$

Since the matrix M had been normalized before the SVD, the command range is 1, and the maximum signed command applicable c_{lim} is $\pm$ 0.5.

Figure 6 shows the maximum peak-to-valley (pv) of the Zernike fit obtained with the three mirrors considered. The Zernikes are ordered according to the OSA/VSIA Taskforce conventions [14]. The rms deformations of the same wavefronts are plotted in Fig. 7a. Figure 7b shows

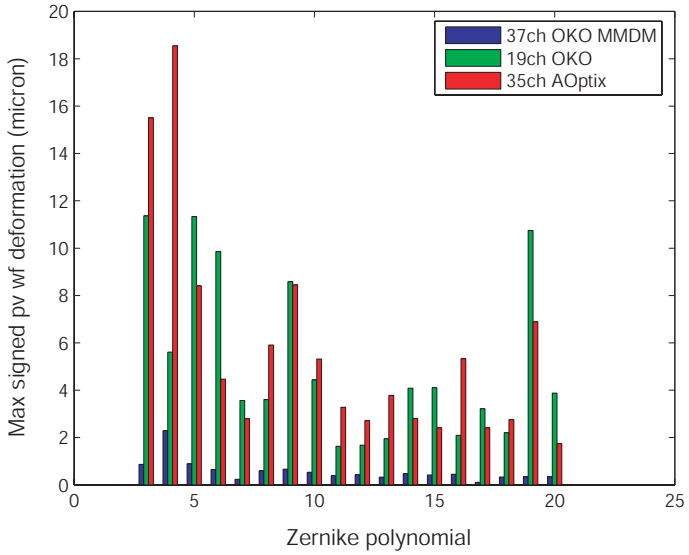

Fig. 6. Comparison of the Zernike generation for the three mirrors in terms of pv signed wavefront produced. The first 21 polynomials are represented (piston, tip and tilt were removed).

the wavefront error for each Zernike fit, calculated as a rms. The peak-to-valley values represent the amplitude of the biggest deformation of the mirror for each considered Zernike, taken as a difference from the minimum and the maximum pixel values. Since these absolute values are calculated from the first saturation of any actuator, they are very sensitive to noise. The rms figures, on the other hand, are calculated from all the pupil values, and can be considered as more representative, even if still affected by noise. Moreover, they are equivalent to the Zernike

#7336 - $15.00 US
Received 3 May 2005; revised 23 May 2005; accepted 23 May 2005

coefficients according to the OSA/VSIA Taskforce, and can be directly related to the wavefront decomposition. The rms errors shall be analyzed along with the maximum rms values, not to over-value them. The rms errors of the AOptix mirror, for example, when related to the Zernike coefficients, are slightly smaller than those of the 37 actuator OKO.

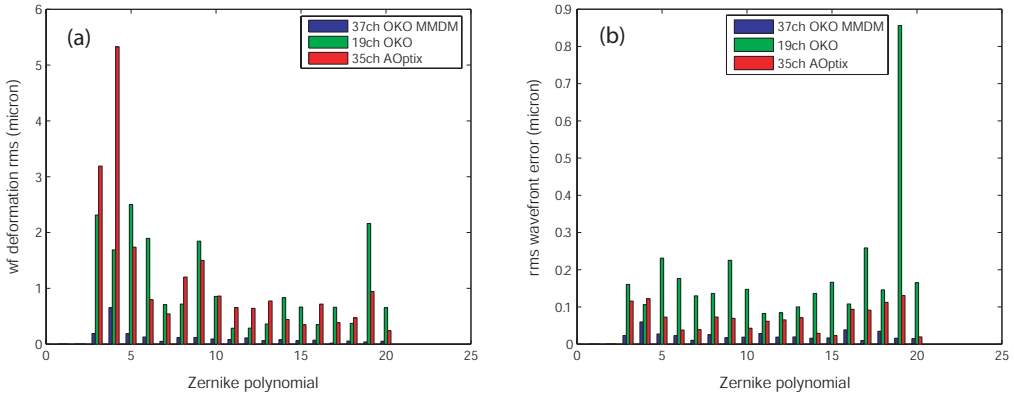

Fig. 7. Comparison of the Zernike generation for the three mirrors: (a) in terms of maximum signed wavefront rms and (b) in terms of residual rms error.

It appears from these plots that the 19 actuator OKO mirror and the 35 actuator AOptix mirror have comparable stroke concerning Zernike generation. The difference arises in the fitting, since the piezoelectric mirror shows a generally higher rms error than the bimorph. The noticeably high value at the Zernike 19, when related to the Zernike rms, is comparable to the other ratios of errors. For both mirrors, the rms error, taken as a ratio of the Zernike fit rms, generally follows a linear increase with the radial order with a higher slope for the piezoelectric mirror. The relatively low performance of the 37 actuator MMDM can be attributed to its limited stroke and the large coupling between actuators. In particular, it can be noted that although the total stroke of the mirror was measured to be 3.5 μm (see Section 2), the simulated defocus signed wavefront deformation (corresponding to the total surface displacement) does not exceed 2.2 μm.

The results presented here are in agreement with previous studies carried out on the 37 actuator OKO and the 35 actuator AOptix mirrors. Fernández *et al.* [5] displayed the range of production of the Zernike polynomials by the 37 actuator OKO mirror, as the total peak-to-valley surface displacement (equivalent to the signed wavefront deformation as presented here). Their calculations were based on simulated IFs of the mirror, which probably can explain why our values are lower (up to 40%). Also, they used only 12 mirror modes to generate these Zernikes. The best appropriate number of modes is usually hard to define, and varies with the application. Using a limited number of modes in our simulations resulted in higher Zernike amplitudes, but also considerably higher rms errors. We decided to further investigate this issue only for the correction typical ocular wavefronts (Subsection 4.2). Regarding Fernández results, the overall same features are nevertheless observed, with a produced defocus term twice as big as the astigmatism terms, and a fast decrease of performance for the higher terms. For the AOptix mirror, the results for the signed Zernike surface displacements (equivalent to half the wavefront deformation) presented by Horsley *et al.* [13] are again consistent with our figures. They first measured the mirror IFs using a phase-shifting interferometer. As they pointed out, the second order terms reach very high values, although the values might be under-estimated when the saturation is only due to one actuator (second term of astigmatism, and first term of trefoil for example in our case). Although the stroke diminishes with the radial order, the signed

#7336 - $15.00 US
Received 3 May 2005; revised 23 May 2005; accepted 23 May 2005

wavefront peak-to-valley still remains above $2\mu m$ for the higher-order aberrations. The same comment can be made on the 19 actuator OKO mirror.

4.2. Correction of typical ocular wavefronts

In order to analyze the performance of a wavefront corrector, it appears more appropriate to fit wavefronts as a whole rather than their decomposition. Indeed, the Zernike decomposition, as any other orthogonal expansion, is useful to describe wavefronts, but is by no means necessary in the correction process. In fact, real adaptive optics control systems do not use Zernike modes. Only an infinite number of Zernike polynomials would represent a complete wavefront base, hence using a limited number induces approximations. The combined mirror performance over the Zernike polynomials might not be representative of its performance over wavefronts as a whole, not only because of these approximations but also because the Zernikes produced by the mirror are no longer orthogonal.

Unlike astronomical adaptive optics, ocular adaptive optics suffers from the lack of knowledge of the statistics of the wavefronts to be corrected. The wavefronts are not spatially stationary and there is no simple theory, such as Kolmogorov theory for turbulence. However there have been several extensive studies (on more than 100 eyes) resulting in some experimental statistics. Thibos *et al.* measured the ocular aberrations of 200 young well-corrected eyes [15] and decomposed the wavefronts over 36 Zernike polynomials. Typical ocular wavefronts can be generated using a MATLAB model containing such statistics as the mean and covariance matrix of the Zernike terms calculated from the measurements [8]. Attention should be paid to the fact that these wavefronts represent well-corrected eyes, meaning that the defocus and astigmatism terms do not exceed 0.25 D. Recalling the previous procedure described, the commands were first calculated using Eq. (3). The vector obtained was modified so that each out-of-range channel was clipped to the maximum value permissible. The final fit phase is given by

$$\Phi_M = UWV^T f(VW^{-1}U^T\Phi) \tag{6}$$

where $f(c_i)$ is the clipping function defined by

$$f(c_i) = \begin{cases} c & \text{if} \quad -c_{lim} \leq c_i \leq c_{lim} \\ c_{lim} \times \frac{c_i}{abs(c_i)} & \text{if} \quad c_i < -c_{lim} \quad \text{or} \quad c_i > c_{lim} \end{cases} \tag{7}$$

If no actuator is out of range, Eq. (6) collapses to the simple projection equation (2).

A sample of 100 generated ocular wavefronts over a 6 mm pupil were processed using these formulae, and the residual rms error after fitting was plotted on Fig. 8. These results were obtained with a reduced number of modes, number which was optimized so that the correction was the best (i.e. lowest rms error). Figure 9 displays the average residual rms error for the same initial wavefronts according to the number of mirror modes used. As was recalled in the last section, the smaller the singular value, the more sensitive the mode. Such "noisy" modes are more likely to make the actuators saturate, and hence degrade the performance of the mirror. This effect is particularly highlighted by the 37 actuator OKO curve, which has a much smaller stroke than the two others as was shown earlier. It is therefore necessary to limit the number of modes used for the calculations. Even though the radial order of correction is reduced, the overall wavefront approximation is better. On the contrary, the 35 actuator AOptix mirror has a sufficient stroke so that the performance improves as more and more modes are used. In fact, a clipping of one of the actuators or more was observed for only 5 wavefronts out of 100. As for the 19 actuator OKO, the figures presented here are in agreement with the analysis performed on the Zernike polynomials: although the stroke of the piezoelectric mirror is comparable to

#7336 - $15.00 US Received 3 May 2005; revised 23 May 2005; accepted 23 May 2005

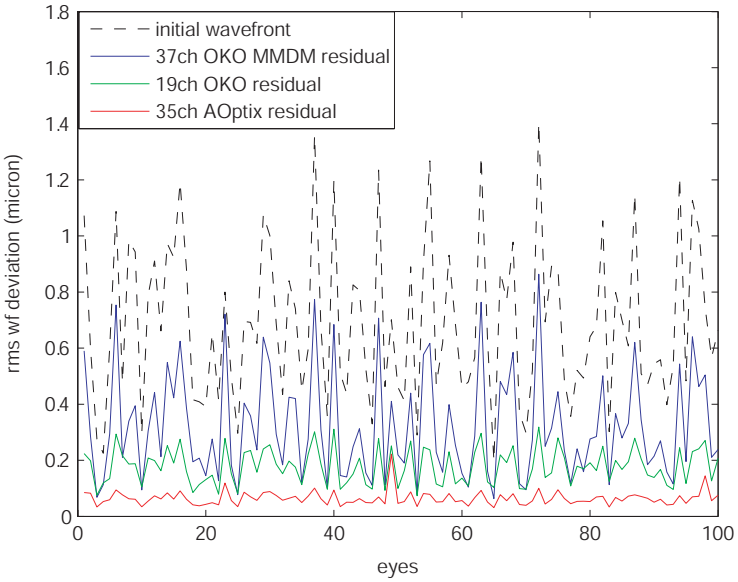

Fig. 8. Residual wavefront rms error after fitting with the three mirrors over a 6 mm pupil. Piston, tip and tilt terms were removed

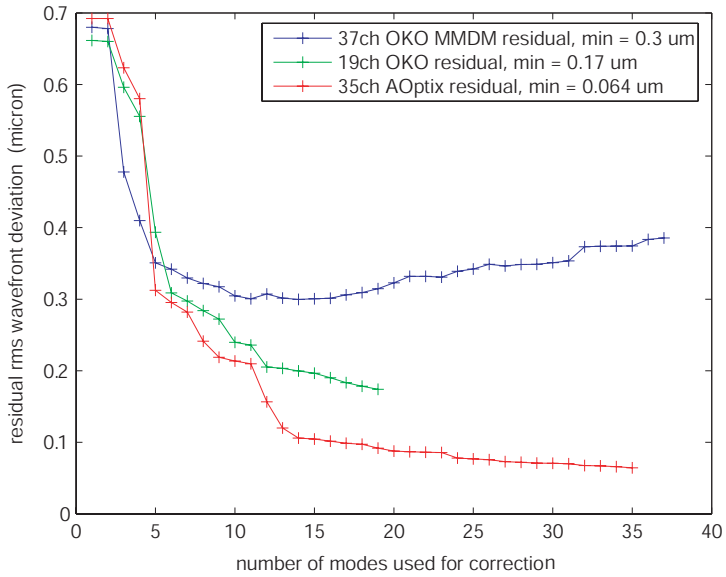

Fig. 9. Residual rms wavefront error after fitting with the three mirrors. The results were averaged from calculations on the same initial wavefronts as in Fig. 8.

the one of the bimorph mirror, the fitting is not as good, probably due to the smaller number of actuators. As was said earlier, the figures plotted were extrapolated from the measurements to simulate the performance of the mirror using the voltage range -150V to +450V. Nevertheless, the performance of the mirror over such typical ocular wavefronts was almost not noticeably affected by a reduction of the range to 0V-300V.

The results presented here are of course ideal calculations. The main assumptions are a per-

#7336 - $15.00 US
Received 3 May 2005; revised 23 May 2005; accepted 23 May 2005

fect actuator response (linear for the 19 actuator OKO and the 35 actuator AOptix mirrors, and quadratic for the 37 actuator OKO MMDM) and a linearly additive effect of the actuators influence functions. Moreover, only the static mirror performance is analyzed here, and the limitations from the wavefront sensor, the noise and the dynamics of the wavefronts are ignored. On the other hand, in a real experimental AO setup, the closed-loop reassessment enables to optimize the correction and handle noise and fluctuations, as well as saturation of the mirror. This last point was further investigated in the particular case of the 37 actuator OKO MMDM which had a serious problem of saturation. The open-loop fitting calculated through Eq. (6) was optimized in a closed-loop fashion such that the residual wavefront was fit again on the mirror modes, and further on. Such a correction loop resulted in the residual rms error following an asymptotic curve converging to the minimum value. A number of 20 iterations was evaluated to give a sufficiently good approximation of the final result. The averaged optimized residual wavefront rms errors are plotted in Fig. 10. The scale used is the same as the one on the previ-

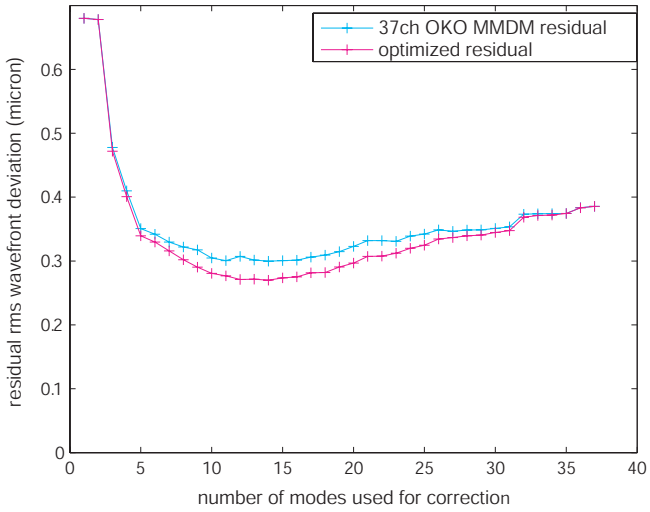

Fig. 10. Comparison of residual rms obtained with an open-loop correction and a closed-loop correction with the 37 actuator OKO MMDM

ous graph so that the comparison can be maintained with the other mirrors. The improvement, although not negligible, does not reach the same level of correction as obtained with the other mirrors.

5. Discussion and conclusion

From the calculations performed, it appears that the AOptix bimorph mirror is the best suited of the three mirrors evaluated for ocular adaptive optics. It demonstrated good ability to generate Zernike polynomials, as well as low rms error when fitting typical ocular wavefronts. The best mean rms error, over 100 generated ocular wavefronts, was 60 nm, which represents only $\lambda/9$ wavefront error in the visible. A very good correction, close to diffraction limit, can be expected in a real control adaptive optics system. Clearly, the simulations reported depend on the appropriateness of the model for the aberrations of the eye. The real performance can only be verified through an experimental set up involving human subjects. In fact, the mirror was implemented in a closed-loop system comprising a Shack-Hartmann sensor. The correction runs showed consistent results, typically a residual rms error of 60 nm for a 4.8 mm pupil. An example is given in Fig. 11. More details concerning the system used and the experimental

#7336 - $15.00 US
Received 3 May 2005; revised 23 May 2005; accepted 23 May 2005

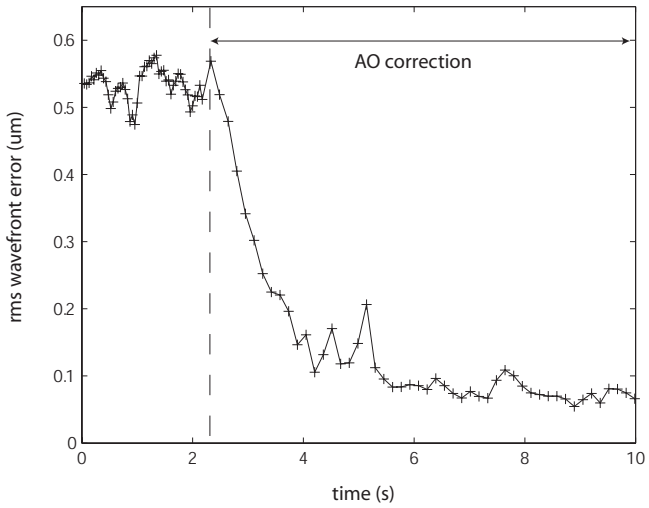

Fig. 11. Closed-loop correction of a human eye with the AOptix mirror (pupil size for measurement: 4.8 mm).

results can be found in the literature [16, 17]. The measurement pupil size was smaller than that used in the simulations, but the various experimental conditions detailed in the previous section explain the slight loss in performance with respect to the predictions. Moreover, it should be noted that the accommodation was not paralyzed, explaining the variations observed. Further experiments increasing the pupil size led to a measured residual rms error of less than 0.1 μm (5.4 mm and 6 mm pupils).

The 37 actuator OKO MMDM showed a problem of saturation resulting in a limited correction, even after static closed-loop optimization of the fitting. It was demonstrated that a larger stroke is necessary, such as that produced by the 19 actuators of the piezoelectric OKO mirror. The latter showed promise, given the actuators number is increased. More simulation work could also be done on this mirror, when varying the optical pupil size to optimize its performance. Finally, attention should be paid to the hysteresis issue and how to deal with it in a control loop to optimize the temporal characteristics.

The methodology described provides a valuable analysis of deformable mirrors for vision science adaptive optics. It enabled to compare the mirrors and point out the appropriate characteristics for such applications, as the technologies are constantly evolving. The same protocol can be used to evaluate new deformable mirrors.

Acknowledgments

We are very grateful to Larry Thibos who provided us with his MATLAB files containing the ocular aberrations statistics as well as the functions to randomly generate a standard eye wavefront, and to Gordon Kennedy for his assistance in using the model.

This research is funded by Science Foundation Ireland under grant number SFI/01/PI.2/B039C and by a European Union EU Research Training Network, contract number HPRN-CT-2002-00301 “SHARP-EYE”.